Research Paper

Investigation of Perforated Tube Configuration Effect on the Performance of Exhaust Mufflers with Mean Flow Based on Three-Dimensional Analysis

Barhm MOHAMAD[(1)*], Jalics KAROLY[(1)], Andrei ZELENTSOV[(2)], Salah AMROUNE[(3)]

[(1)] *Faculty of Mechanical Engineering and Informatics, University of Miskolc*
Miskolc, Hungary
*Corresponding Author e-mail: pywand@gmail.com

[(2)] *Piston Engine Department, Bauman Moscow State Technical University*
Moscow, Russia

[(3)] *Université Mohamed Boudiaf*
M'sila, Algérie

Using perforated tube in exhaust mufflers is known to improve transmission loss (TL) by improving their sound pressure level (SPL) at the orifice. The perforated tube should affect the muffler performance analogous to a shell-and-tube heat exchanger. To the authors' knowledge, there are few previous assessments reported in literature of the effects that the perforated tube configuration has on acoustic response and pressure drop predicted. The effects of (i) the perforated tube length, (ii) the diameter of tube holes, and (iii) flow through perforated tube were investigated. To assess the perforated tube effect on flow, the SOLIDWORKS 2017 based on Computational Fluid Dynamics (CFD) tool was utilized using real walls approach model with a surface roughness of 0.5 micrometres (AISI 316 cold rolled stainless steel sheet (ss) $Ra = 0.5$ μm). Perforated tube was found to cause back pressure which may increase SPL about 10%.

Keywords: exhaust muffler; finite element method; acoustic characteristics; flow characteristics; optimization.

1. Introduction

Hybrid mufflers reduce the exhaust noise through their volume depending on the reflection of sound waves and absorbing coefficient, used for all range of frequencies (Mohamad, 2019). Mohamad *et al.* (2020) investigated the effect of perforated tube dimensions on the sound pressure level. A numerical prediction was made by Elsayed *et al.* (2017) to improve the transmission loss of the muffler by analyzing the position and size of perforated tube inside the reactive muffler. The interior sound quality can be used to differentiate vehicles or brands as well as give an overall impression of the quality of the vehicle. Siano (2010) investigated the noise attenuation characteristics of a typical perforated muffler using 1D and 3D commercial software. In order to account for the effect of mean flow that exists inside the muffler, a three-dimensional

Finite Element Method (3D FEM) is used in conjunction with the Computational Fluid Dynamics (CFD) simulation of the flow field. More concretely, the 3D mean flow field is computed by firstly using CFD, and then the obtained mean flow data are imported to an acoustic solution undertaken using AVL Boost. The data transfer between the two steps is accomplished by mesh mapping. In general, increasing flow velocity increases the SPL and decreases the resonance peaks.

Lee and Selamet (2006) studied the influence of perforated impedance on the acoustic performance of reflective and resistive mufflers using experimental and computational approaches. The Boundary Element Method (BEM) was applied for the prediction of Transmission Loss (TL) in dB of mufflers with different perforation geometries. Different duct porosities ($\alpha = 8.4$ and 25.7%), hole diameters ($D_h = 0.249$ and 0.498 cm), and fiber filling densities ($\rho_f = 100$

and 200 kg/m^3) were utilized to illustrate the effect of such parameters on the TL of mufflers. Demir and Çinar (2009) and Tiryakioglu (2020) studied a similar problem in the case where acoustic waves in an infinite and semi-infinite cylindrical duct system by applying Wiener-Hopf technique to demonstrate the effect of the outer duct radius, the contrast of the lining impedances, the mean flow, and the acoustical impedance of the central perforated tube on the sound propagation. The aim of this study is to find out the effects of porosity value, the perforated tube length and the diameter of tube holes inside the muffler on the acoustic behaviour of the race car muffler.

2. The influence of surface roughness of stainless steel on absorbing noise

The material used in this silencer is an austenitic stainless-steel type (AISI 316), and is considered non-magnetic, highly resistant to corrosion, which starting powder is gas atomised, and has a maximum particle size of 22 μm. This steel has a homogenous microstructure with a homogeneous core in the surface, which enables high quality surface finishes and machining to be obtained. This steel is suitable for galvanic treatments as well as chemical and physical deposits. Its chemical composition is given in Table 1.

Table 1. Chemical composition of AISI316.

$\%\text{C}^{(1)}$	<0.03
$\%\text{Mn}^{(2)}$	<2
$\%\text{P}^{(2)}$	<0.01
$\%\text{S}^{(1)}$	<0.005
$\%\text{Si}^{(2)}$	<1
$\%\text{Cr}^{(2)}$	16–19
$\%\text{Ni}^{(2)}$	9–13
$\%\text{Mo}^{(2)}$	1.5–3
$\%\text{N}^{(2)}$	<0.003
$\%\text{O}^{(2)}$	<0.002
$\%\text{Fe}$	Compl.

Fig. 1. FS muffler.

3. Physical model and computational procedure

Engine scheme was made by one-dimensional gas dynamics code based on finite volume method for simu-

lating engine cycle performance. It is widely used by automotive and exhaust manufacturers. CFD simulations were performed using SolidWorks 2017 to assess the effect of the perforated tube on the flow. Solid-Works is an open source CFD solver based on control volume discretization. Compressible steady state was assumed. In addition, the following data was measured from race car workshop: the wall temperature of an external pipe was set $T_w = 573$ K, heat transfer coefficient $h_c = 50 \text{ W/m}^2/\text{K}$ and ambient temperature 300 K.

Inlet velocity: 40 m/s, inlet temperature: 400 K, inlet pressure: 120 000 Pa, outlet pressure (atmospheric): 101325.00 Pa, outlet temperature (atmospheric): 293.2 K, all internal walls were set as real walls with a surface roughness of 0.5 micrometres (AISI 316 cold rolled stainless steel sheet (ss) $Ra = 0.5 \text{ μm}$).
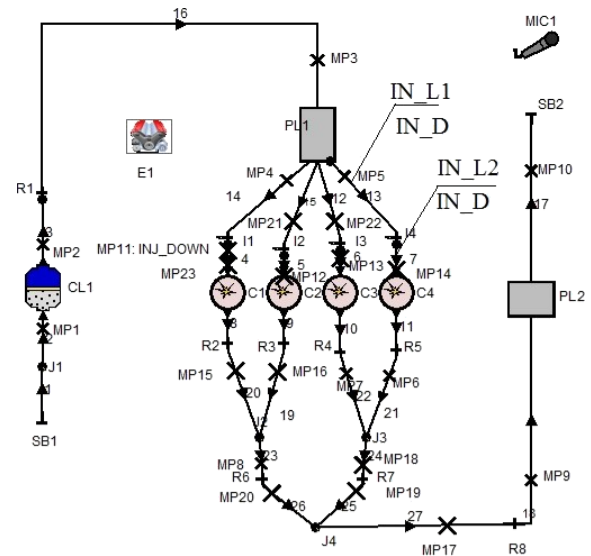
Fig. 2. 1D model of the Honda CBR 600RR (PC 37) engine: volume of muffler chamber (PL2) (Mohamad *et al.*, 2019).
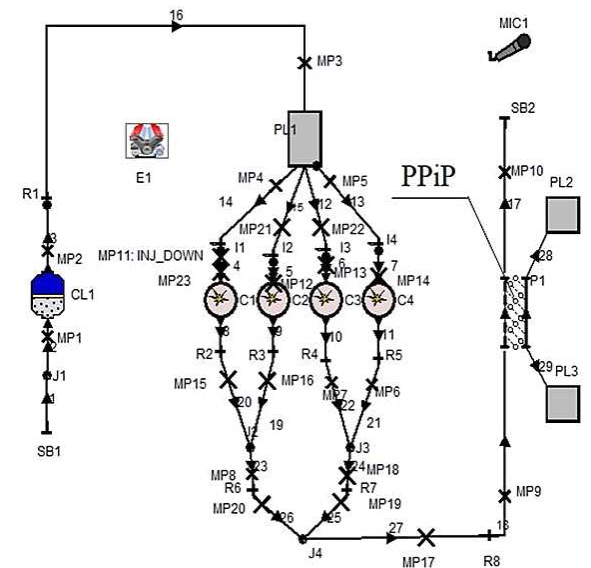
Fig. 3. Engine scheme: modified parameters – perforated pipe inside pipe (PPiP) (Mohamad *et al.*, 2020).

4. Numerical procedure

In virtually every measure of comparison, realizable $(k - \varepsilon)$ demonstrates a superior ability to capture the mean flow of the complex structures. The compressible continuity is described by the following equation (FERZIGER, PERIC, 2002):

$$\frac{\partial(\rho u)}{\partial x} + \frac{\partial(\rho v)}{\partial y} + \frac{\partial(\rho w)}{\partial z} = 0. \qquad (1)$$

Momentum is described by the following formula

$$\frac{\partial}{\partial x}(\rho_i \rho_j) = -\frac{\partial p}{\partial x_i} + \frac{\partial}{\partial x_j}\left[\mu\left(\frac{\partial u_i}{\partial x_j} + \frac{\partial u_j}{\partial x_i}\right)\right]$$
$$- \frac{\partial}{\partial x_j}(\overline{\rho u_i u_j}). \qquad (2)$$

Transport for the turbulence energy generation and dissipation rates are described by the following equations:

$$\frac{\partial(\rho k u_j)}{\partial x_j} = \frac{\partial}{\partial x_j}\left[\left(\mu + \frac{\mu_t}{\sigma_k}\right)\frac{\partial k}{\partial x_j}\right]$$
$$+ G_k + G_b - \rho_\varepsilon - Y_m - S_k, \qquad (3)$$

$$\frac{\partial}{\partial x_j}(\rho\varepsilon u_j) = \frac{\partial}{\partial x_j}\left[\left(\mu + \frac{\mu_t}{\sigma_\varepsilon}\right)\frac{\partial \varepsilon}{\partial x_j}\right] + \rho C_1 S\varepsilon$$
$$- \rho C_2 \frac{\varepsilon^2}{k + \sqrt{v\varepsilon}} + C_{1\varepsilon}\frac{\varepsilon}{k}C_{3\varepsilon}G_b + S_\varepsilon, \quad (4)$$

where G_k represents the rate generation of turbulent kinetic energy (TKE) which arises due to mean velocity gradients, G_b is the rate generation of turbulent kinetic energy which arises due to buoyancy, Y_m represents the fluctuating dilation in compressible turbulence that contributes to the overall dissipation rate, S_ε and S_k are source terms defined by the user, and p is sound pressure

$$\nabla\left(\frac{1}{\rho_o}\nabla p\right) + \frac{k^2 p}{\rho_o} = 0, \qquad (5)$$

where $k = 2\pi f/c_o$ is the wavelength, ρ_o is the density of the air, and c_o is the speed of sound.

5. Transfer Matrix Method (TMM)

As a technique for simulating the acoustic transfer characteristic, the transfer matrix method, which defines the principle of impedance, was applied. This approach, which is widely used for acoustic systems because of its computational simplicity, makes design simple because each element is modelled separately.

Considering acoustic pressure, p, and mass velocity, u, as the two state variables in the transfer matrix method, the results from the four-pole parameters from the conditions of both sides, which can be describe as

Eq. (6), where $[p_r, u_r]^T$ is called the state vector at the upstream point, r and $[p_{r-1}, u_{r-1}]^T$ are called state vector at the downstream point $r - 1$ (SIM *et al.*, 2008)

$$\begin{bmatrix} p_r \\ u_r \end{bmatrix} = \begin{bmatrix} \text{transfer matrix} \\ 2 \times 2 \end{bmatrix}\begin{bmatrix} p_{r-1} \\ u_{r-1} \end{bmatrix}. \qquad (6)$$

The transmission loss is independent of the source and presumes an anechoic termination at the downstream end. It is defined as the difference between the power incident on the acoustic element and that transmitted downstream into an anechoic termination. So, it makes the evaluation and prediction easy to leave the reflected pressure due to radiation impedance out of consideration. The transmission loss is an energy loss of acoustic elements, so the ratio of sound pressure between the inlet and outlet of acoustic elements can be expressed in dB scale.

6. Mesh generation and mesh sensitivity analysis

Concerning the one-dimensional approach, the AVL Boost code was utilized. It is able to reproduce in the time-domain the sound pressure level occurring inside the device, under the hypothesis of a planar pressure wave propagation. The muffler is schematized as a network of pipes, coupled together by junctions of different types. The flow equations are then solved within each pipe following a finite-volume method. The solution of the flow equations, particularly in the first section and last section of the muffler, finally allows to estimate SPL ratio. The accuracy of the numerical results hardly depends on a correct 1D schematization of the engine. 1D scheme may be very difficult to realize for complex geometries, like in the case of a three-pass perforated muffler. Geometrical details and 3D effects can be better taken into account in Finite Element Method (FEM) and Boundary Element Method (BEM) (CUI *et al.*, 2014). For this reason, in the following, the SOLIDWORKS code was also utilized. Obviously, in this case a 3D grid of the whole device had been previously built with a proper cell size, affecting the accuracy of the results at high quality mesh.

The 1D and 3D predicted SPL profiles are compared and discussed in order to assess the potentiality and limitations of the employed numerical approaches. In each case, the influence on the acoustic performance of variations in the flow velocity, is analyzed as well. Figure 4 shows the generated CFD mesh, which is fine and dense, and the mesh near to the walls is densified further in order to resolve the boundary layer.

Although requiring high computational and memory resources, it allows to account for higher order modes that cannot be accurately described using one-dimensional modelling technique. Figure 4 displays the whole 3D domain, including the details of its internal
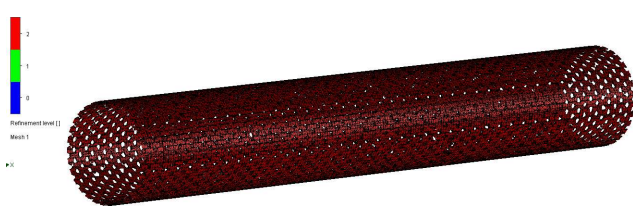
Fig. 4. Refinement mesh applied for perforated tube.

geometry, with the presence of perforated tube, located within the expansion chamber. The model consists of 140173 solid cells and 76776 fluid cells. For the chosen mesh size, a tetrahedral mesh can be used, still preserving a good accuracy of the results.

7. Results

7.1. The effect of perforated inner tube on the flow characteristics

In the absence of experimental data, the matching between 1D and 3D results also represent an indirect validation of the numerical data. Moreover, very similar findings are reported in the (Mohamad et al., 2020). Visualized pressure fields at 2000 rpm were 101 983.68 Pa and dropped to 101 087.29 Pa at the end of muffler, as the flow indicator arrows show in the Fig. 5.
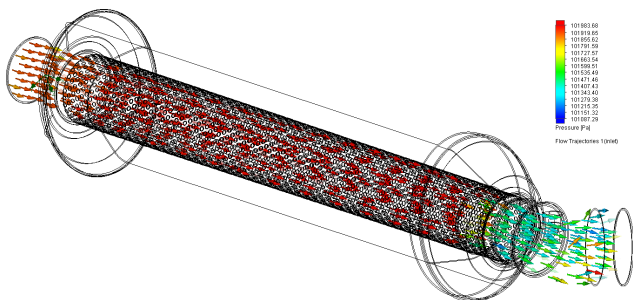
Fig. 5. Pressure contour for the straight-through perforated pipe.

7.2. Flow distribution without perforated part

The flow velocity inside circular tube shows that there are an infinite number of pulses produced. With he more continuous the exhaust flow, a fast moving pulse creates a low pressure area behind it. Figure 6 shows the velocity variation through different zones in geometry. It is found higher in the constrained pipe about 64.272 m/s.

A pressure-based solver was calculated to visualise flow characteristics and identify critical zone for the muffler. The pressure field in this case was obtained through software inbuilt pressure solver, which solves interlinked continuity and momentum equation. The
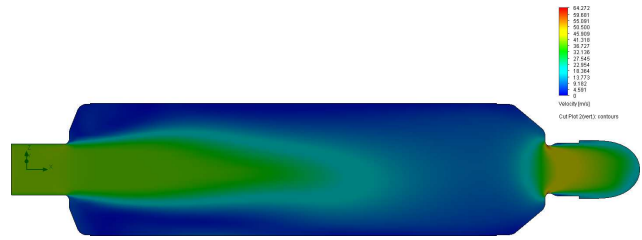
Fig. 6. Velocity contour inside the muffler chamber without perforated pipe, starting from the left side (inlet) to right side (outlet).

reference values were computed from the left side (inlet) as show in Fig. 7.
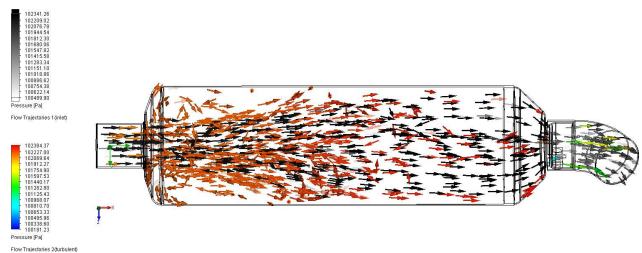
Fig. 7. Pressure contour inside the muffler chamber without perforated pipe start from the left side (inlet) to right side (outlet).

The maximum pressure was 102 384.37 Pa and the minimum was 100 181.23 Pa observed in the muffler chamber in turbulent state without perforated tube. The maximum pressure at the inlet pipe and muffler tail was 102 341.26 Pa and minimum was 100 489.90 Pa. The internal pressure of the expansion chamber is relatively stable, and the distribution is relatively uniform. It can be concluded that one cause of a significant reduction in pressure between the two parts (PPiP and chamber) is that the airflow through the inner tube creates a greater pressure. Mutations in the gas flow cross-section can have a greater pressure loss. If the flow direction and the gas flow conditions change with a greater degree, it not only will generate the eddy current phenomenon, but also consume more energy.

7.3. The effect of muffler dimensions on the sound pressure level

The results of this part of the investigation are presented in form of curves of sound pressure level in decibels plotted against diameter of the inner tube holes. The order noise radiated from the orifice of the exhaust systems is caused by the pressure pulses generated by the periodic charging and discharging process and propagated to the open ends of the duct systems. The curves were calculated using theory of transfer matrix method. Figure 8 clearly shows the requirement for damping the pulse result from engine exhaust gas.
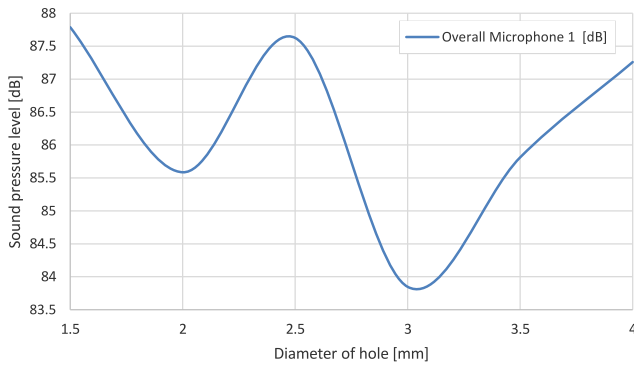
Fig. 8. The effect of diameter of hole [mm] of perforated pipe inside the muffler on sound pressure level, SPL [dB].

7.4. The effect of length on the sound pressure level

The effect of varying the length of the muffler on the sound pressure level is shown in Fig. 9. The peak SPL for length 406 mm was 88 dB, the lowest SPL calculated for length 436 mm was about 84 dB. The effect was not so significant for engine speed 2000 but it could be significant for higher engine speed due to the higher flowrate of exhaust gas.
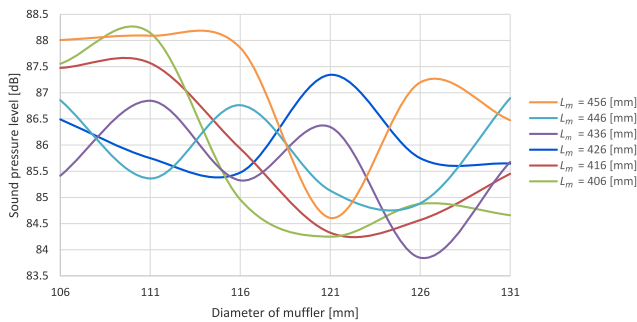
Fig. 9. Results of variation of pipe length L_m and diameter D_{m_out} of non-perforated outer pipe (diameter of perforated inner pipe D_{m_in} = 47 mm, n = 2000 rpm) on sound pressure level, SPL.

7.5. Muffler Transmission loss and back pressure analysis

Transmission loss was calculated for three porosity values (0.29, 0.6 and 0.9) on a similar model as shown in Fig. 10. For acoustic FEM analysis, Johnson-
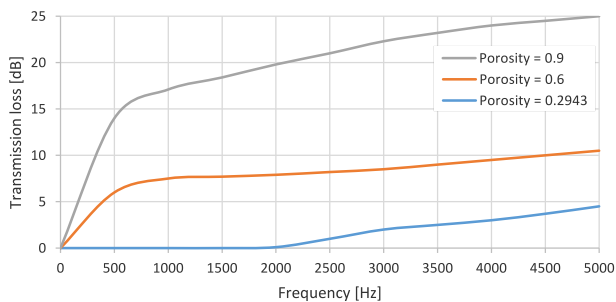
Fig. 10. Transmission loss at different frequencies and different porosities.

Champoux-Allard model (JCA) was used for porous medium. However, TL for the basic (current) hole diameter of the FS muffler at high porosity appears to diminish, which is in agreement with LEE and SELAMET (2006).

For the same porosity back pressure was calculated using CFD analysis. Steady and compressible flow was carried out with heat transfer. $K - \varepsilon$ model was used for turbulent analysis.

Table 2. Back pressure at different porosities.

Porosity	0.29	0.6	0.9
Back pressure [mbar]	889	821	795

8. Conclusions

The current research investigated the poor performance of the Honda CBR 600RR (PC 37) race car engine which resulted in extensive modifications, the complete rebuild of an engine with performance camshafts and free flow manifolds. The numerical results illustrate that the effect of different hole diameters with the same porosity on the TL is more significant at lower duct porosities. It is also observed that varying the diameter of the holes affects the SPL of the hybrid muffler with the same porosity and muffler diameter. Results are encouraging but they also point out that there is a problem with the muffler chamber size: a two-element device, one per bank. Current investigations lead to conclusion that the issue revolves around the point where the two zones join at their outputs, leading to turbulence which is causing excessive low frequency noise at rpm below 3000, despite a new performance exhaust system.

This work reveals characteristics of exhaust mufflers based upon linear flow of gases at their input and thus concludes that excessive turbulence will result in ineffective silencing/muffling.

References

1. CUI F., WANG Y., CAI R.C. (2014), Improving muffler performance using simulation-based design, [in:] *INTER-NOISE and NOISE-CON Congress and Conference Proceedings*, **249**(7): 1190–1194.

2. DEMIR A., ÇINAR Ö.Y. (2009), Propagation of sound in an infinite two-part duct carrying mean flow inserted axially into a larger infinite duct with wall impedance discontinuity, *ZAMM – Journal of Applied Mathematics and Mechanics*, **89**(6): 454–465, doi: 10.1002/zamm.200800145.

3. ELSAYED A., BASTIEN C., JONES S., CHRISTENSEN J., MEDINA H., KASSEM H. (2017), Investigation of baffle configuration effect on the performance of exhaust mufflers, *Case Studies in Thermal Engineering*, **10**: 86–94, doi: 10.1016/j.csite.2017.03.006.

4. Ferziger J.H., Perić M. (2002), *Computational Methods for Fluid Dynamics*, 3rd ed., Springer, doi: 10.1007/978-3-642-56026-2.

5. Lee I., Selamet A. (2006), Impact of perforation impedance on the transmission loss of reactive and dissipative silencers, *The Journal of the Acoustical Society of America*, **120**(6): 3706–3713, doi: 10.1121/1.2359703.

6. Mohamad B. (2019), Design and optimization of vehicle muffler using the Ffowcs Williams and Hawkings model, *Machine Design*, **11**(3): 101–106, doi: 10.24867/MD.11.2019.3.101-106.

7. Mohamad B., Karoly J., Zelentsov A., Amroune S. (2020), A hybrid method technique for design and optimization of Formula race car exhaust muffler, *International Review of Applied Sciences and Engineering*, **11**(2): 174–180, doi: 10.1556/1848.2020.20048.

8. Siano D. (2010), Three-dimensional/one-dimensional numerical correlation study of a three-pass perforated tube, *Simulation Modelling Practice and Theory*, **19**(4): 1143–1153, doi: 10.1016/j.simpat.2010.04.005.

9. Sim H.J., Park S.G., Joe Y.G., Oh J.E. (2008), Design of the intake system for reducing the noise in the automobile using support vector regression, *Journal of Mechanical Science and Technology*, **22**(6): 1121–1131, doi: 10.1007/s12206-008-0306-z.

10. Tiryakioglu B. (2020), Radiation of sound waves by a semi-infinite duct with outer lining and perforated end, *Archives of Acoustics*, **45**(1): 77–84, doi: 10.24425/aoa.2020.132483.